# 0.1–10 MeV Neutron Soft Error Rate in Accelerator and Atmospheric Environments

Matteo Cecchetto, Rubén García Alía, *Member, IEEE*, Frédéric Wrobel, Andrea Coronetti, *Student Member, IEEE*, Kacper Bilko, David Lucsanyi, Salvatore Fiore, *Member, IEEE*, Giulia Bazzano, Elisa Pirovano, and Ralf Nolte

***Abstract*— Neutrons with energies between 0.1 and 10 MeV can significantly impact the soft error rate (SER) in SRAMs manufactured in scaled technologies, with respect to high-energy neutrons. Their contribution is evaluated in accelerator, ground-level, and avionic (12 km of altitude) environments. Experimental cross sections were measured with monoenergetic neutrons from 144 keV to 17 MeV, and the results benchmarked with Monte Carlo simulations. It was found that even 144 keV neutrons can induce upsets due to elastic scattering. Moreover, neutrons in the 0.1–10 MeV energy range can induce more than 60% of the overall upset rate in accelerator applications, while their contribution can exceed 18% in avionics. The SER due to neutrons below 3 MeV, whose contribution has always been considered negligible, is found to be up to 44% of the total upsets in accelerator environments. These results have strong radiation hardness assurance (RHA) implications for those environments with high fluxes of neutrons in the 0.1–10 MeV energy range.**

***Index Terms*— Accelerator, avionics, COTS SRAM, ground-level, intermediate-energy neutrons, low-energy neutrons, SEU cross sections.**

## I. Introduction

NEUTRONS are the primary particles constituting the radiation environment inside the large hadron collider (LHC) accelerator at CERN. Their fluxes can be tens of times higher than the broad mixed field of protons, electrons, muons, pions, and kaons that together characterize the locations of the accelerator where electronics are installed. In this framework, neutrons are the main threat for electronics in terms of inducing single-event effects (SEEs), of which single-event upsets (SEUs) are discussed in this work. Furthermore, neutrons are also the main concern for ground-level and avionic applications, as once produced in the atmosphere, due to their nature, they can travel until interacting with atoms in semiconductor devices. Both accelerator and atmospheric environments are characterized by a wide neutron spectrum, from thermal (25 meV) up to several GeV of energies. In the accelerator context, high-energy hadrons (HEHs) are defined as neutrons, protons, pions, and kaons with energies above 20 MeV. The SEU response of electronic components, such as SRAMs, is assumed to be in saturation above 20 MeV [1]. Below this threshold, the SEU contribution due to charged hadrons, including the effects of the proton direct ionization, can be neglected in most of the cases as far as accelerator applications are concerned [1], [2].

In regards to the neutron SEU response, in addition to the aforementioned HEH fluence, intermediate-energy neutrons defined between 0.2 and 20 MeV are taken into account, weighting their differential fluence with the Weibull function of a reference SRAM memory [2]. This approach to characterize the SEU sensitivity of electronics is defined as the HEH equivalent (HEHeq) fluence [reported in terms of fluence from [3] in (1)], for which the Toshiba TC554001AF (400 nm) memory is considered as reference response. Note that the same equation can be expressed in terms of average flux [$\mathrm{cm}^{-2}/\mathrm{s}$]

$$\Phi_{\mathrm{HEHeq}} = \int_{0.2\mathrm{MeV}}^{20\mathrm{MeV}} w(E) \cdot \frac{d\Phi_n(E)}{dE}\, dE + \int_{20\mathrm{MeV}}^{+\infty} \frac{d\Phi_{\mathrm{HEH}}(E)}{dE}\, dE. \quad (1)$$

In (1), $w(E)$ is the Weibull response to intermediate-energy neutrons from 0.2 to 20 MeV, and $d\Phi_n(E)/dE$ and $d\Phi_{\mathrm{HEH}}(E)/dE$ are the neutron and HEH differential fluences, respectively. The energy threshold of 0.2 MeV was set to consider the lowest onset energy for the $(n, \alpha)$ inelastic reactions of neutrons and materials typically present in microelectronics (in this case nitrogen that can be used as a dopant, as well as in insulating materials [1]). However, as it will be shown in this work, elastic processes can also deposit enough energy in submicron technologies to trigger SEUs for energies even below 0.2 MeV. In the following, low-energy neutrons are defined as those neutrons below the lowest energy threshold for inelastic reactions that produce charged particles

Manuscript received December 9, 2020; revised January 26, 2021; accepted February 10, 2021. Date of publication March 9, 2021; date of current version May 20, 2021. This work was supported in part by the European Union's Horizon 2020 Research and Innovation Program under MSC Agreement 721624.

Matteo Cecchetto is with CERN, CH-1211 Genève, Switzerland, and also with the Université de Montpellier, IES-UMR UM/CNRS 5214, F-34097 Montpellier, France (e-mail: matteo.cecchetto@cern.ch).

Rubén García Alía, Kacper Bilko, and David Lucsanyi are with CERN, CH-1211 Genève, Switzerland.

Frédéric Wrobel is with the Université de Montpellier, IES-UMR UM/CNRS 5214, F-34097 Montpellier, France.

Andrea Coronetti is with CERN, CH-1211 Genève, Switzerland, and also with the Department of Physics, University of Jyväskylä, 40014 Jyväskylä, Finland.

Salvatore Fiore and Giulia Bazzano are with ENEA, Department of Fusion and Nuclear Security, Frascati Research Center, 00044 Rome, Italy.

Elisa Pirovano and Ralf Nolte are with the Department of Physikalisch-Technische Bundesanstalt, 38116 Brunswick, Germany.

Color versions of one or more figures in this article are available at https://doi.org/10.1109/TNS.2021.3064666.

Digital Object Identifier 10.1109/TNS.2021.3064666

in $^{28}$Si, which is 2.75 MeV for $(n, \alpha)$ reactions. However, this definition does not include thermal neutrons.

The ground-level spectrum has high fluxes of neutrons below 10 MeV, and the sensitivity of electronics to this fraction of spectrum has increased in nanometer technologies, as previously shown in [4]. Indeed, the technology scaling leads to a general reduction of the energy threshold $E_{\text{th}}$ in SRAMs and FPGAs, with a ratio as low as 10 between saturated and 2.5 MeV neutron SEU cross sections, for the most sensitive parts presented in [5]. Therefore, the contribution to the soft error rate (SER) from neutrons between 1 and 10 MeV has been recently investigated. In this regard, the minimum energy threshold currently imposed at 10 MeV in the JESD89 standard has been discussed to be shifted down to 1 MeV [6]. In the atmospheric environment, it was shown [7] that neutrons below 10 MeV can induce up to 13% of SEUs in 65 nm SRAMs and [5] reports a contribution of 10%. For power MOSFETs, the SEEs in the relative 1–10 MeV range are reported to be up to 19% in [6], and in addition, it was concluded that the current $E_{\text{th}}$ in the JEDEC standard should not be shifted down to 1 MeV, because it would lead to a higher measurement error comparable to the SER increase. The relative impact of several energy ranges of 1–3, 1–10, and 1–20 MeV neutrons on the SER in accelerator and ground-level applications is detailed in [8], for SRAMs and FPGAs down to 65 nm. It was found that the 1–10 MeV neutron contribution to the SER in accelerator applications can be more than five times larger than that in atmospheric environments, yielding a non-negligible contribution up to 37% in the case of the FPGA. This was mainly due to the high intermediate-energy neutron fluences with respect to HEH fluences. Moreover, albedo neutrons (energies below 10 MeV) can also increase the SER in 45 and 28 nm technologies up to a factor of 20% in the former [9], [10].

In this framework, this study continues the work presented in [8], with a broad collection of experimental data on state-of-the-art SRAMs tested with monoenergetic neutrons from 144 keV to 17 MeV. It is worth to note that access to such beams (and hence publications of related results) is quite rare for electronic applications. The memories were tested with the package and delidded to assess its impact on the SEU cross section. The SER due to neutrons between 0.1 and 10 MeV is computed for ground-level, avionic (12 km), and accelerator environments, including a soft and hard spectrum reproduced in the CERN High energy AcceleRator Mixed-field (CHARM) facility. SEU results have been benchmarked with those calculated from a model through Monte Carlo simulations. In addition, the study is performed also for neutrons in the 0.1–3 MeV range, whose contribution has always resulted negligible in previous publications [5], [8]. The SER retrieved by applying the current memory response is compared to the events obtained from the HEHeq approximation, evaluating whether it can be still considered as valid.

## II. SRAM Components and Test Facilities

### A. Tested Components

The devices under test (DUTs) are commercial off-the-shelf (COTS) SRAMs of different node sizes, because of their high interest for accelerator applications. Table I reports the characteristics of the ISSI 40 nm, Cypress 65 nm, and Cypress 90 nm memories, which can be hereafter referred to as ISSI, Cypress 65, and Cypress 90, respectively. These memories, powered at nominal voltage of 3.3 V, are written and read through a motherboard tester developed at CERN and the SEU count is retrieved. The setup can also detect multiple bit upsets (MBUs), but none or just a few of them were observed during the tests. In addition, the ESA SEU reference monitor is employed, which is a golden chip to benchmark the measurements between facilities.

TABLE I
SPECIFICATIONS OF THE SRAMS STUDIED IN THIS WORK

| Memory | Reference | Date code | Tech. | Size [Mbit] |
|---|---|---|---|---|
| ISSI | IS61WV204816BLL-10TLI | 1650 | 40 nm | 32 |
| Cypress | CY62167GE30-45ZXI | 1731 | 65 nm | 16 |
| Cypress | CY62157EV30LL-45ZSXI | 1843 | 90 nm | 8 |
| ESA Monitor | AT68166H-YM20-E | 1817 | 250 nm | 16 |

The tested SRAMs, with same reference and date code, were irradiated both with their package and delidded in some cases. The delidding (or decapsulation) consists in removing part of the top package of the memory via specific techniques, in order to directly expose its sensitive area to radiation. The ESA Monitor was tested without lid. All devices were irradiated at normal beam incidence and from the top side of the memory package.

### B. Test Facilities

Intermediate-energy neutron measurements were performed at the accelerator facility PIAF of the Physikalisch-Technische Bundesanstalt (PTB), the national metrology institute of Germany, and in the Frascati Neutron Generator (FNG) at the ENEA Frascati Research Centre (Italy). In both facilities, the target is located at several meters of distance from walls, floor, and ceiling, in order to minimize as much as possible the neutron scattering.

PTB can provide a very broad set of monoenergetic neutron energies, from 24 keV up to 19 MeV [11]. Table II reports the complete list of neutron energies (En) used for our tests, with the corresponding reactions, in the form Target (Projectile, Ejectile), and projectile energy. For instance, neutrons of 0.144 MeV are produced by the interaction of 1.943 MeV protons with a lithium target, and they were used to assess the sensitivity of the SRAMs below the assumed threshold of 0.2 MeV. In addition, the distance of DUT to the target and the corresponding average flux during the tests are included (the latter reported as the highest among different runs). To notice that 2.5 MeV neutrons, tested in both facilities for comparison, are produced through different reactions. Furthermore, tritium in the Ti(T) target used for the 17 MeV can decay in $^{3}$He and produces protons with the incoming deuteron beam via the $^{3}$He(d, p)T reaction. In order to stop these protons (maximum energy of 17 MeV), an aluminum foil of 0.5 mm was interposed between the beam and DUT.

TABLE II
NEUTRON REACTIONS PRODUCED IN PTB AND FNG, WITH CORRESPONDING PROJECTILE ENERGY, CLOSEST DISTANCE OF DUT TO THE TARGET AND AVERAGE FLUX, BOTH DURING THE TESTS

| Facility | $E_n$ [MeV] | Reaction | $E_{proj}$ [keV] | d [cm] | $\varphi_n$ [$cm^{-2}/s$] |
|---|---|---|---|---|---|
| PTB | 0.144 | Li(p,n) | 1943 | 5.5 | $4.0 \cdot 10^5$ |
| PTB | 1.2 | T(p,n) | 2047 | 5.5 | $1.8 \cdot 10^6$ |
| PTB | 2.5 | T(p,n) | 3356 | 5.5 | $1.9 \cdot 10^6$ |
| FNG | 2.5 | D(d,n) | 300 | 2.5 | $3.8 \cdot 10^6$ |
| PTB | 5 | D(d,n) | 2406 | 6.6 | $8.2 \cdot 10^5$ |
| PTB | 8 | D(d,n) | 2524 | 6.6 | $2.7 \cdot 10^6$ |
| FNG | 14.8 | T(d,n) | 300 | 2.5 | $1.2 \cdot 10^8$ |
| PTB | 17 | T(d,n) | 1264 | 5.5 | $5.2 \cdot 10^5$ |

Detailed information about the neutron production and relative fields in PTB is presented in Section II-C.

FNG was originally designed for experiments on thermonuclear fusion and it is also available for electronics testing. A deuteron beam is accelerated in a target, either containing tritium, producing 14 MeV neutrons through the $T(d,n)\alpha$ reaction or deuteron, which provides 2.5 MeV neutrons according to the $D(d,n)^3He$ fusion reaction [12].

In addition to the neutron tests, the SEU cross sections were measured with 18.6 and 29 MeV protons in the Terapia Oncologica con Protoni - Intensity Modulated Proton Linear Accelerator for Radio Therapy (TOP-IMPLART) LINAC (Frascati, Italy), and with 40, 50, 80, 124, 164, and 184 MeV protons in the Kernfysisch Versneller Institute (KVI, The Netherlands). In both facilities, tests were performed in air. TOP-IMPLART is a linear accelerator currently providing 35 MeV protons, which are degraded with a lead foil to obtain lower energies. The accelerator is under construction with the final aim of providing 150 MeV for proton therapy applications [13]. KVI can provide primary energies of 190, 66.5, or 30 MeV which are degraded with aluminum slabs [14].

### *C. Monoenergetic Beams and Neutron Production in PTB*

A neutron field or beam produced by a nuclear reaction is monoenergetic if the neutron energy is a unique function of the neutron emission angle under ideal conditions, that is, mass-less DUT and negligible energy loss of the projectile in the reactive layer. This requires that the nuclear reaction has exactly one exit channel with only two particles and no excited states involved.

Under realistic conditions, however, the energy distribution of the monoenergetic neutron produced at a given emission angle exhibits a finite width which reflects the energy loss of the projectile in the reactive target layer. In addition, these "monoenergetic" neutrons are accompanied by neutrons of lower energy which result from scattering of primary "monoenergetic" neutrons in the DUT. Usually, experimental conditions are selected such that the relative width of the energy distribution of the monoenergetic neutrons and the relative contribution of scattered neutrons are only a few percent each.

If the kinematic conditions mentioned above are not met, that is, several exit channels are possible, the resulting neutron field is called quasi-monoenergetic even if the monoenergetic exit channel is dominating. In such cases, the monoenergetic component is accompanied by lower energy neutrons resulting from other reaction channels, for example, breakup reactions of the target or projectile nuclei with more than two particles in the exit channel. This is typical when producing neutron energies above 20 MeV through the $^7Li(p,n)^7Be$ reaction, resulting in a spectrum composed of a main peak and a lower energy tail [15].

At the PTB ion accelerator facility PIAF, monoenergetic neutron fields with mean neutron energies at 0° between 144 keV and 8 MeV and between 14.8 and 19 MeV are produced using the nuclear reactions $^7Li(p,n)^7Be$, $^3H(p,n)^3He$, $^2H(d,n)^3He$, and $^3H(d,n)^4He$. The deuteron beam energy employed for producing the 8 MeV field using the $^2H(d,n)^3He$ reaction is already above the threshold for the breakup reaction $^2H(d,np)^2H$, which corresponds to a neutron energy of 7.70 MeV for the monoenergetic channel $^2H(d,n)^3He$. However, the breakup cross section at this energy is so small that the field is practically monoenergetic. In the energy region between 8 and 14.8 MeV, no useful monoenergetic neutron producing reaction is available. In this energy region, the neutron energy distributions produced by bombarding deuterium targets with deuterons always exhibit a monoenergetic component and a more intense breakup component at lower energies [16].

Hence, only neutrons in the energy region 144 keV to 8 MeV and 14.8 to 19 MeV are monoenergetic and can be employed to investigate the sensitivity of electronics.

As discussed above, the neutron energy distributions at the position of the DUT are composed of the primary monoenergetic beam and the spectrum of neutrons scattered in the target assembly. This contribution was calculated through simulations provided by the facility (considering a disk of 1 $cm^2$) and resulted in less than 4% with respect to the main neutron fluence (1.1% at 144 keV). The cutoff energy in these simulations was 2 keV.

Thermal neutrons (around neutron energy of 25 meV) are not produced with the primary neutron field and are only part of the room-return background that results from neutron thermalization in the walls. However, the large dimensions of the hall and the low-mass grid floor are specifically designed to reduce as much as possible the neutron room return, thus thermal neutron fluxes at the DUT position are negligible.

## III. MONOENERGETIC LOW–INTERMEDIATE-ENERGY NEUTRON AND PROTON CROSS SECTIONS

The first neutron tests were carried out at FNG, where the ISSI memory was shown to have the 2.5 MeV SEU cross section only six times lower than that in saturation (considering 184 MeV protons at KVI). Subsequently, the same devices were measured in PTB, where a broader range of low- and intermediate-energy neutrons is provided, with the aim of obtaining a better picture of the sensitivity of these memories as a function of the neutron energy. In this regard, the memories were also tested delidded (i.e., without the package) with

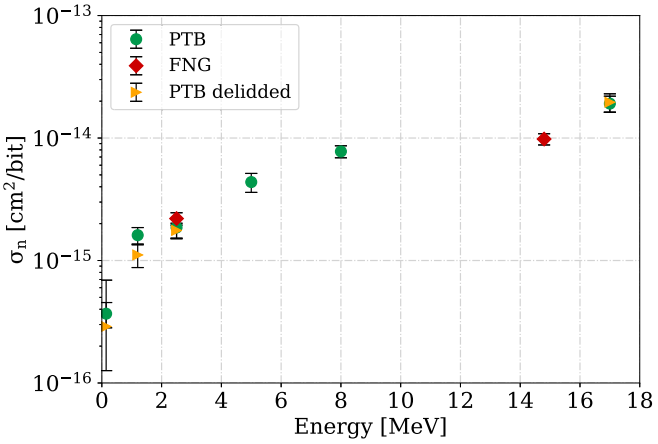


Fig. 1. ISSI 40 nm neutron cross sections, measured at FNG and PTB. Comparison with the delidded memory for some energies. Error bars are reported with 95% of confidence level, including statistical and fluence uncertainties.

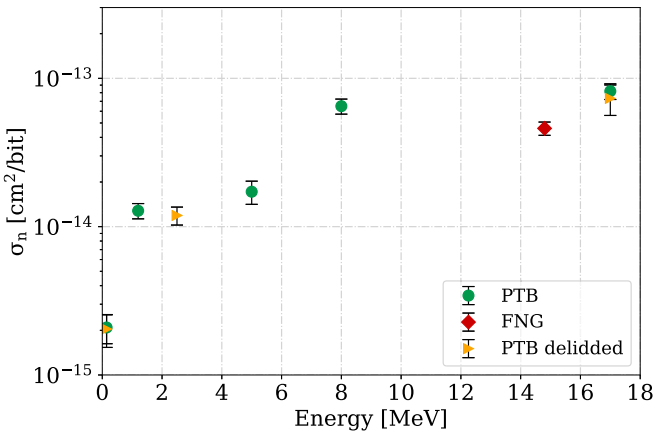


Fig. 2. Cypress 65 nm neutron cross sections, measured at FNG and PTB. Comparison with the delidded memory for some energies. Error bars are reported with 95% of confidence level, including statistical and fluence uncertainties.

some energies. Indeed, as shown in [17], the neutron cross section below 10 MeV of SRAMs can increase because of elastic interactions with the H atoms composing the package. These protons, which are ejected mainly in the same direction of the incoming beam [17], can reach the sensitive area of the device, and therefore, contribute to increasing the SEU cross section. In fact, the memories studied in this work are sensitive to low-energy protons [2].

The neutron SEU cross section measurements at FNG and PTB are shown in Figs. 1–3 for the ISSI, Cypress 65, and Cypress 90 memories and ESA Monitor, respectively. In addition, the delidded SEU cross sections are included in the same plots. Error bars include the contribution of count statistics and fluence uncertainties, which are summed in quadrature, with a confidence level of 95%. The statistical uncertainty is calculated from the number of measured upsets ($N$), which are modeled as a Poisson distribution with standard deviation $2\sigma_{\text{stat}} = 2\sqrt{N}$ ($N > 50$). The fluence uncertainty, considered to be $2\sigma_{\text{fluence}} = \pm 10\%$, is provided by the facility and assessed through the ESA Monitor, which shows the map homogeneity of the beam over a surface of $19.8 \times 19.8$ mm$^2$.

As can be seen, for the ISSI and Cypress 65 memories, the package does not have a significant impact on the SEU cross sections. Table III reports the SEU cross section values at the energy extremes: low- and intermediate-energy neutrons at 0.144, 1.2, and 17 MeV from PTB and high-energy protons measured at 184 MeV in KVI for the ISSI and Cypress 65 memories, and at 150 and 200 MeV in PSI for Cypress 90 memory (different date code) and ESA Monitor, respectively.

The ISSI and Cypress 65 memories show a relatively high cross section even at 1.2 MeV with respect to the saturated value, measured with 184 MeV protons. For instance, the Cypress 65 neutron cross section at 1.2 MeV is only six times lower than the high-energy proton value in saturation (see Table III). The complete set of ratios between high-energy proton and neutron cross sections are shown in Fig. 4, for the four memories. Even at 0.144 MeV, that is, below the energy threshold of 0.2 MeV (so far considered the lowest onset energy to calculate the HEHeq fluence for the SEU estimation), the ISSI and Cypress 65 memories did not show a completely negligible SEU cross section, which is 38 and 37 times lower than the saturated values, respectively (see Fig. 4). To further verify that neutrons of such low energies

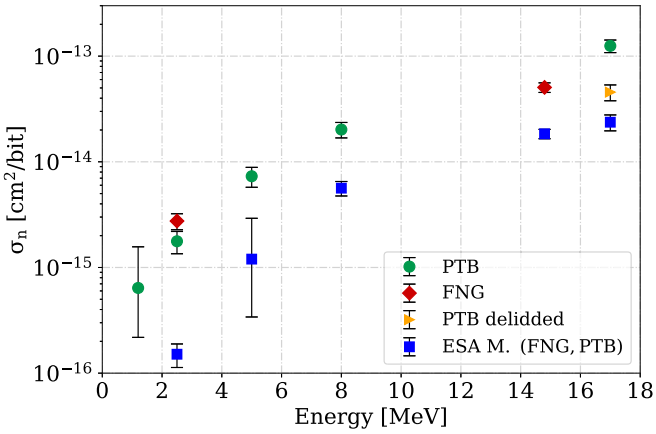


Fig. 3. Cypress 90 nm 8 Mbit and ESA Monitor neutron cross sections, measured at FNG and PTB. Comparison with the delidded memory at 17 MeV. Error bars are reported with 95% of confidence level, including statistical and fluence uncertainties.

TABLE III
LOW-ENERGY NEUTRON (0.144, 1.2 MEV), 17 MEV NEUTRON, AND HIGH-ENERGY PROTON SATURATED SEU CROSS SECTIONS FOR THE TESTED MEMORIES AND THEIR RATIO BETWEEN HIGH AND LOW ENERGIES

| Memory | $\sigma^n_{0.144}$ [cm$^2$/bit] | $\sigma^n_{1.2}$ [cm$^2$/bit] | $\sigma^n_{17}$ [cm$^2$/bit] | $\sigma^p_{sat}$ [cm$^2$/bit] | $\frac{\sigma^p_{sat}}{\sigma^n_{1.2}}$ |
|---|---|---|---|---|---|
| ISSI 40 | $3.68 \cdot 10^{-16}$ | $1.61 \cdot 10^{-15}$ | $1.91 \cdot 10^{-14}$ | $1.40 \cdot 10^{-14}$ | 8.7 |
| Cypress 65 | $2.09 \cdot 10^{-15}$ | $1.28 \cdot 10^{-14}$ | $8.19 \cdot 10^{-14}$ | $7.73 \cdot 10^{-14}$ | 6 |
| Cypress 90 | - | $6.40 \cdot 10^{-16}$ | $1.25 \cdot 10^{-13}$ | $2.13 \cdot 10^{-13}$ | 333 |
| ESA M. | - | - | $2.37 \cdot 10^{-14}$ | $2.60 \cdot 10^{-14}$ | - |

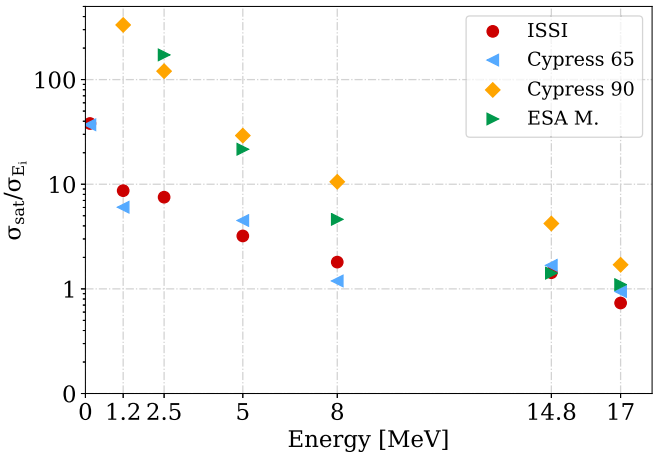


Fig. 4. Ratio between high-energy proton (saturated) and neutron SEU cross sections. The data for both the ISSI and Cypress memories are from the measurements with the package.

can still indirectly deposit enough energy to trigger an SEU, simulations were carried out, and the results will be shown in Section VII.

Moreover, thermal neutron effects on low-energy neutron measurements are excluded, as the fields produced in PTB are monoenergetic, the spectra of neutrons scattered in the DUT are not composed of thermal neutrons, and the neutron background is negligible. Additional confirmation of this fact can be done considering the thermal neutron cross sections of the same SRAMs, which were measured in a nuclear reactor (ILL [18]). Given the low thermal neutron SEU cross section, for instance of the Cypress 65 memory ($4.91 \cdot 10^{-16}$ cm$^2$/bit), very large fluxes would be needed in order to have a significant overall impact.

The cross sections of Cypress 90 and ESA Monitor memories behave according to what was previously assumed, with SEU cross section ratios between high energy and neutrons below 2.5 MeV in the order of several hundreds (see Fig. 4). Therefore, the sensitivity of the ISSI 40 nm and Cypress 65 nm memories is still significant at low energies and, as it will be shown, this aspect plays a significant role on the contribution to the overall SER of neutrons below 10 MeV.

Furthermore, for the Cypress 65 and ISSI SRAMs, the 17 MeV neutron cross section (from Table III) is higher than that measured with high-energy protons, by 6% and 36%, respectively. In addition, the 17 MeV SEU cross sections are almost a factor of 2 higher than those at 14.8 MeV, and the energy points are solely 2.2 MeV apart. For these memories, the SEU cross section has already reached the saturation for energy as low as 8 MeV.

A Weibull function is adopted to fit the experimental data of each memory and the corresponding parameters are reported in Table IV. According to the cross section shape, the energy threshold is set to be 0.01 MeV for the ISSI and Cypress 65 memories, 0.1 MeV for Cypress 90 memory, and 0.2 MeV for the ESA Monitor. Even if some memories showed a higher cross section at 17 MeV than with higher proton energies, the latter is kept as saturation cross section.

TABLE IV

WEIBULL FIT PARAMETERS OF THE TESTED MEMORIES AND THE TOSHIBA REFERENCE FOR THE HEHEQ CALCULATION (FROM [1])

| Memory | $\sigma_{sat}$ [cm$^2$/bit] | $E_{th}$ [MeV] | W [MeV] | s |
|---|---|---|---|---|
| ISSI 40 nm | $1.40 \cdot 10^{-14}$ | 0.01 | 14.05 | 0.82 |
| Cypress 65 nm | $7.73 \cdot 10^{-14}$ | 0.01 | 11.57 | 0.80 |
| Cypress 90 nm | $2.16 \cdot 10^{-13}$ | 0.1 | 24.22 | 1.98 |
| ESA M. 250 nm | $2.60 \cdot 10^{-14}$ | 0.2 | 13.08 | 2.99 |
| Toshiba 400 nm | $6.60 \cdot 10^{-14}$ | 0.2 | 9.25 | 3.02 |

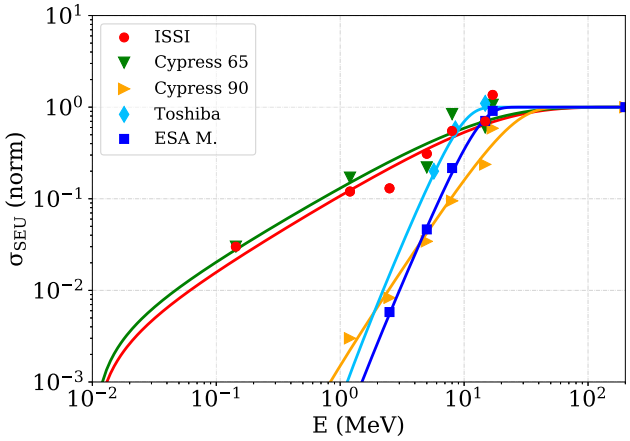


Fig. 5. Weibull functions of the tested memories and experimental SEU cross sections normalized to 1. The Toshiba curve is the standard response so far employed for the HEHeq calculation.

In the Weibull calculation, the neutron measurements and the saturated proton cross section were considered, excluding the 17 MeV data when higher than the saturated value. As shown in the following, this choice is supported by measurements performed with a neutron spectrum up to 11 MeV, produced by an americium–beryllium source, as well as SEU cross section simulations.

Fig. 5 shows the experimental SEU cross sections and the respective Weibull fits normalized to 1. In addition, the Weibull response of the Toshiba memory, employed as a reference SRAM for computing the HEHeq fluence, is added on the plot for comparison from [1].

## IV. ADDITIONAL INTERMEDIATE-ENERGY NEUTRON MEASUREMENTS WITH AN AMERICIUM–BERYLLIUM SOURCE

Aiming at further quantifying the sensitivity of the SRAM components to intermediate-energy neutrons, an americium–beryllium (Am–Be) source was employed. In this case, a continuous spectrum of neutrons is used to perform SEU cross section measurements. The source, located at CERN, has an activity of 888 GBq which provides an isotropic neutron flux of $5.03 \cdot 10^7$ [n/s]. The neutron spectrum has a peak around 3 MeV and reaches a maximum energy of 11 MeV, as shown in the FLUKA [19]–[21] simulation of Fig. 6 (from [22]).

As introduced, the HEHeq fluence depends on the memory response, which is described through a Weibull function,

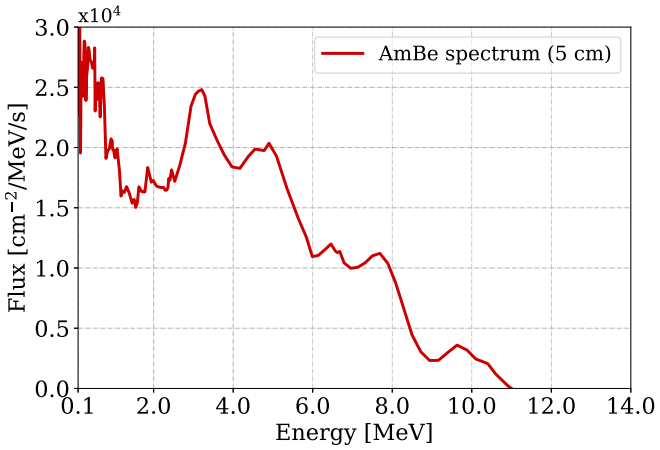


Fig. 6. Americium–beryllium neutron spectrum at 5 cm (test position). The source is located at CERN and provides a maximum energy of 11 MeV.

TABLE V

AM–BE SEU MEASUREMENTS VERSUS SEU ESTIMATION FROM THE WEIBULL RESPONSES OF THE MEMORIES. THE HEHEQ FLUXES ARE REFERRED TO THE TESTS PERFORMED AT 5 CM FROM THE CENTER OF THE SOURCE. FOR COMPARISON, THE HEHEQ FLUX OF THE TOSHIBA REFERENCE IS $1.84 \cdot 10^4$ CM$^{-2}/s$

| Memory | HEHeq flux [cm$^{-2}$/s] | $N_{measured}$ [SEU/Mbit/day] | $N_{calculated}$ [SEU/Mbit/day] |
|---|---|---|---|
| ISSI 40 nm | $4.0 \cdot 10^4$ | 39 | 42 |
| Cypress 65 nm | $4.6 \cdot 10^4$ | 209 | 322 |
| ESA Monitor | $9.8 \cdot 10^3$ | 21 | 22 |

TABLE VI

SEU CROSS SECTIONS OF MEMORIES WITH PACKAGE AND DELIDDED, MEASURED WITH THE AM–BE NEUTRON SOURCE

| Memory | $\sigma_{package}$ [cm$^2$/bit] | $\sigma_{delidded}$ [cm$^2$/bit] | $\frac{\sigma_{package}}{\sigma_{delidded}}$ |
|---|---|---|---|
| ISSI 40 nm | $1.33 \cdot 10^{-14}$ | $1.36 \cdot 10^{-14}$ | 0.97 |
| Cypress 65 nm | $5.01 \cdot 10^{-14}$ | $4.79 \cdot 10^{-14}$ | 1.05 |
| Cypress 90 nm | $1.64 \cdot 10^{-13}$ | $1.64 \cdot 10^{-13}$ | 1.00 |

as can be seen in Table V (reported in terms of flux for a direct comparison). The expected upset rate in [SEU/Mbit/day] is computed by weighting the differential fluence of the Am–Be source with the memory's Weibull response (from Table IV) and compared to that experimentally measured. Results are reported in Table V, showing an excellent agreement regarding ISSI and ESA Monitor data. For Cypress 65, this assessment is less accurate, with an expected upset rate higher by roughly 50% than the measured one. This difference can mainly be attributed to deviations between the Weibull fit and the actual response function. The agreement was worse when the 17 MeV saturated cross sections were used to calculate the Weibull functions, hence this supports the choice of using the proton SEU cross sections in saturation.

In addition, the memories were measured with the package and delidded. However, as shown in Table VI, there is not a significant difference between the resulting SEU cross sections, which are calculated by applying to the Am–Be spectrum the corresponding Weibull function of each memory, to retrieve the HEHeq fluence.

## V. SER INDUCED BY NEUTRONS IN THE 0.1–10 MEV ENERGY RANGE

The SER of the SRAM devices due to neutrons in the 0.1–10 MeV energy range is evaluated in atmospheric and accelerator environments. The New York City (NYC) sea-level neutron spectrum is calculated with the mathematical model from the JEDEC (JESD89A) standard [23], and the ground level-like spectrum from the ChipIr facility is added for completeness from [8]. In addition, the neutron spectrum at typical flight altitudes (12 km) is added to the analysis. The latter is calculated above Geneva from simulations based on FLUKA and extracted through the MAIRE tool [24]. Regarding accelerator environments, the RR spectrum is that of a lightly shielded alcove in the LHC (40 cm of cast iron/concrete). In fact, a large quantity of electronic devices is installed inside these shielded alcoves, which are parallel to the LHC tunnel. Moreover, G0 and R10 spectra are produced in the CHARM facility at CERN and they resemble the main radiation environments found in the LHC accelerator [25]. These mixed-field spectra are characterized by a soft and hard spectrum, respectively. In the calculation, both G0 and R10 are composed of neutrons, protons, and pions above 20 MeV and only of neutrons below this energy, as the contribution of other particles to the SER is negligible below 20 MeV. The differential spectra of these environments are depicted in Fig. 7 for energies above 1 MeV, normalized to the JEDEC NYC integrated flux above 10 MeV and corresponding to a fluence of $1.13 \cdot 10^5$ [$n$/cm$^2$/year]. The same spectra are shown in lethargy units in Fig. 8, highlighting the differences in the 1–10 MeV neutron fluxes for the various environments. As can be seen, the spectra shape below 10 MeV are visibly different, the accelerator fluxes being several times higher than that of the JEDEC standard. Neutrons at flight altitude (12 km) present instead lower fluxes between 1 and 10 MeV, while they have a harder spectrum (even more than the accelerator ones) at high energies.

The SER is calculated integrating the differential spectrum of the considered environment folded with the Weibull response of each memory (as it was done for the Am–Be neutron environment in Section IV). Therefore, SEUs are counted starting from the energy threshold of the Weibull functions (of Table IV), which is different between memories. For ease of notation, this lower energy limit will be referred to as 0.1 MeV. The present analysis aims to compare intermediate- to high-energy neutrons, while the effects of thermal neutrons in these memories was studied in [26]. Fig. 9 shows the fraction of upsets (in percentage) induced by neutrons with energy between 0.1 and 10 MeV on the overall rate, for the SRAM memories and different environments. The Cypress 90 nm SEU results are analogous to those of the ESA Monitor, hence they are represented by the latter. As expected from the neutron SEU cross section response, the Cypress 65 nm has the highest relative upset rate in all the environments. In ground-level

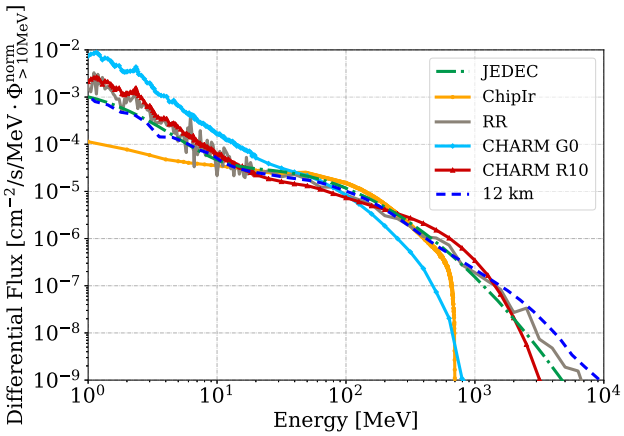


Fig. 7. Differential spectra above 1 MeV normalized to the JEDEC NYC neutron flux above 10 MeV. The neutron spectrum at 12 km of altitude is compared to the ground-level one. G0 and R10 represent a soft and more energetic mixed field found in the CHARM facility, mainly composed of neutrons. RR is the actual spectrum of a shielded alcove inside the LHC.

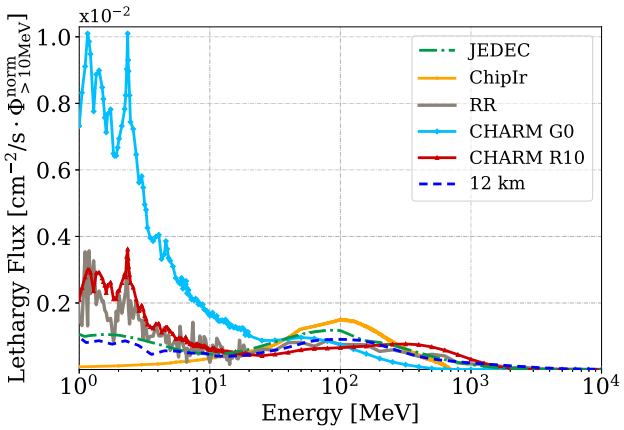


Fig. 8. Lethargy spectra (linear $y$-axis) above 1 MeV normalized to the JEDEC NYC neutron flux above 10 MeV. The neutron spectrum at 12 km of altitude is compared to the ground-level one. G0 and R10 represent a soft and more energetic mixed field found in the CHARM facility, mainly composed of neutrons. RR is the actual spectrum of a shielded alcove inside the LHC.

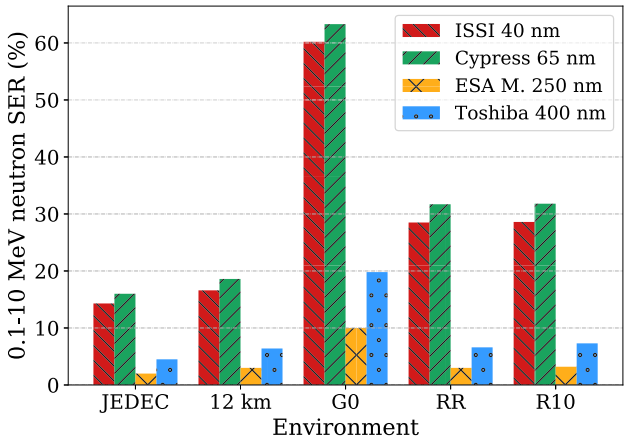


Fig. 9. SER induced by the fraction of neutrons between 0.1 and 10 MeV (in percentage) on the total upset rate, for the different technological nodes of SRAM memories and in the ground-level, avionic, and accelerator environments.

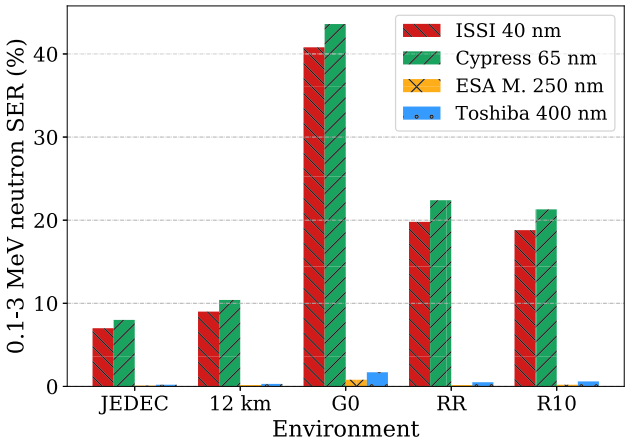


Fig. 10. SER induced by the fraction of neutrons between 0.1 and 3 MeV (in percentage) on the total upset rate, for the different technological nodes of SRAM memories and in the ground-level, avionic, and accelerator environments.

applications, the SEU rate due to neutrons below 10 MeV is up to 16% of the total, whereas it can be larger for avionic applications at 12 km of altitude, up to 19%. In accelerator environments, the contribution is more critical, reaching up to 63% of the failure rate with a soft spectrum such as G0 and 32% with the more energetic environments in R10 and the RR alcove. The ISSI 40 nm memory has also a similar SER to that of Cypress 65 nm, while the older technologies, 250 nm ESA Monitor, 400 nm Toshiba, and 90 nm Cypress memories show a negligible impact for most of the applications, and in any case not exceeding 20%. Despite the very large Cypress 65 and ISSI cross sections at 1.2 MeV, the neutron flux in that region at ground level is not high enough to yield a considerable SEU contribution, although their relative upset rate is three times higher than that with older technologies. Conversely, in some accelerator environments, the flux below 10 MeV is considerably higher than that at higher energies (see Fig. 8) and the large Cypress 65 cross section at low energy provides a non-negligible contribution to the SER.

The same analysis is performed for neutrons in the 0.1–3 MeV range and the relative SER is depicted in Fig. 10. Surprisingly, this range of neutrons, which were considered negligible even for accelerator environments [8], can yield a considerable failure rate in the two most sensitive SRAMs. Up to 44% of upsets are induced in the Cypress 65 memory with a soft accelerator spectrum (G0) and 22% with a harder one (RR). At 12 km of altitude, up to 10% of SEUs can be induced. Comparing these results to the SER below 10 MeV, it can be noticed that neutrons between 0.1 and 3 MeV can have a stronger contribution than neutrons between 3 and 10 MeV. This occurs because the sensitivity of the memories to low-energy neutrons is very high, and the environment fluxes are larger at lower energies. This aspect is well depicted in Fig. 10, where the less sensitive memories (ESA Monitor and Toshiba) exhibit a totally negligible contribution.

Extending the analysis below 1 MeV for the Cypress 65 memory, the contribution is negligible in atmospheric environments (<5%) and provides an SER of 21% and 13% in G0 and RR, respectively. The failure rate

TABLE VII
RATIO BETWEEN HEHEQ FLUENCES CALCULATED THROUGH THE CYPRESS 65 AND TOSHIBA MEMORY RESPONSES IN G0 AND RR, CONSIDERING THE FLUENCE OF THE ENVIRONMENT UNTIL 10 AND 20 MEV AND THE FULL SPECTRUM

| Spectrum | $\frac{\text{HEHeq(Cypress65)}}{\text{HEHeq(Toshiba)}}$ | | |
|---|---|---|---|
| | <10 MeV | <20 MeV | Full |
| G0 | 6.22 | 3.02 | 1.95 |
| RR | 6.21 | 2.50 | 1.29 |

is about 1% for energies below 0.1 MeV (without considering thermal neutrons). In addition, the fact of assuming the lower energy threshold for the HEHeq fluence calculation of 0.2 MeV [see (1)], instead of 0.01 MeV, yields a worst case SER underestimation of 3.4%. Hence, the 0.2 MeV limit can still be considered, in general, valid, as the contribution of neutrons below this threshold is negligible.

To summarize, in some accelerator locations, neutrons in the 0.1–10 MeV energy range can induce more than 60% of the total SEUs and 44% derive from neutrons between 0.1 and 3 MeV. Regarding terrestrial and avionic applications, the relative failure rate below 10 MeV is 16% and 18%, respectively. It can typically be neglected for noncritical devices, but the technology scaling and increasing of sensitivity to low-energy neutrons pose some threats also in these environments.

## VI. HEHEQ FLUENCE UNDERESTIMATION AND RHA IMPLICATIONS

As a consequence of the previous analysis, the 400 nm Toshiba response employed as reference in the HEHeq calculation (and implemented in FLUKA) can no longer be considered the worst case response, and the 65 nm Cypress memory shows a greater relative contribution from intermediate-energy neutrons. The underestimation of the Toshiba reference with respect to the Cypress 65 nm memory is quantified by calculating the ratio between the respective HEHeq fluences from (1), and the results are shown in Table VII. The HEHeq fluences are calculated considering the G0 and RR spectra for energies from 0.1 MeV until 10 and 20 MeV and the full spectrum. As can be seen, the underestimation in the 0.1–10 MeV range is a factor larger than 6 for both the soft spectrum (G0) and the harder environment (RR). Furthermore, considering the complete intermediate-energy range between 0.1 and 20 MeV and the full environment spectrum, the previous underestimation is up to a factor of 3 and 2, respectively. The latter value is more meaningful as the operational environment is composed of the full energy spectrum, but the other ratios provide an estimation for potential LHC environments with softer spectra than G0. It is to be noted that the underestimation of the HEHeq fluence will be directly reflected on the SER.

Consequently, these aspects have important radiation hardness assurance (RHA) implications, and three solutions are presented.

1) The HEHeq fluence can be calculated with the current Toshiba reference response of the RadMon and a safety margin of two can be applied to the HEHeq fluence. However, this approach can be valid for those accelerator environments presenting a harder spectrum than that in G0, from which the fluence underestimation is calculated. Otherwise, the safety margin must be larger, as seen in the examples of Table VII.
2) For a worst case scenario, the Cypress 65 memory should be employed instead of the Toshiba reference in the HEHeq fluence calculation. This approach is more accurate than solution 1 and would work with softer spectra than that of G0. However, it relies on the knowledge of the neutron spectrum in the area of interest, which is not always the case.
3) Both solutions 1 and 2 may lead to an overestimation of the estimated SER for cases in which the memory concerned is not particularly sensitive to intermediate-energy neutrons. The ideal solution would be to fully characterize the component with several intermediate neutron energies, as performed for the present work, but owing to different factors (time constraints, facility availability, costs, and so on), this is not always practically feasible. To overcome this difficulty, a more realistic possibility is to qualify the device with 2.5 MeV neutrons, in addition to the high-energy protons, whose energy is available in several facilities and is low enough to assess the sensibility of the memory at low energies. In fact, as seen in Section III, the SEU cross section measured at 14 MeV (and even at 8 MeV) is still comparable to its value in saturation. From the ratio between the high-energy proton and 2.5 MeV neutron SEU cross sections, it is instead evident that whether the memory is very sensitive to low-energy neutrons or not. As shown in Fig. 4, if this ratio is above 100, the memory will not be particularly sensitive to low energies, hence the SER estimation can be performed by using the Toshiba response. Differently, when the ratio is around 10, the memory will be considerably sensitive to low-energy neutrons and the Cypress 65 memory response can be employed instead. For intermediate values of the ratio, the relation to estimating the SER is not straightforward, but a possible solution would be to vary the Weibull function of a reference memory (for instance, the Cypress 65), until matching with the 2.5 MeV cross section of the new device (normalized to the reference). This action can be performed by varying the $s$ and $E_{\text{th}}$ parameters of the Weibull fit, which determine most of the horizontal shift of the function.

## VII. NEUTRON AND PROTON SIMULATIONS

With the aim of better understanding the behavior of the Cypress 65 and ISSI memories that, as opposed to previous technologies, show a large sensitivity to low-neutron energies, the respective SEU cross sections were calculated through Monte Carlo simulations. In addition, simulations can confirm that, at such low energies (0.144, 1.2 MeV), neutrons can elastically interact with atoms and indirectly deposit the required energy to trigger an SEU. Monte Carlo simulations have been performed using the G4SEE application

based on Geant4 toolkit (version 10.6.p01) [27]. G4SEE has been developed at CERN to obtain the event-by-event direct and indirect energy deposition histograms, in micrometric electronic component volumes for studying SEEs. Regarding the Geant4 physics models [28], [29], for proton simulations, *G*4HadronElasticPhysics hadron elastic models and FTFP_BERT hadron inelastic models were used. The latter mainly uses the Geant4 Bertini intranuclear cascade model at the energies relevant for these studies. In the case of neutrons below 20 MeV, the HP High Precision neutron models and cross sections were used for both elastic and inelastic scattering. G4Em StandardPhysics_option4 was added too, which is the combination of the best and most precise electromagnetic models, needed for the direct energy deposition. Cross section biasing has also been applied for elastic and inelastic interactions of primary protons and neutrons, to enhance the CPU performance of the simulations. Moreover, the application permits to disentangle the energy deposition between inelastic and elastic processes. A preliminary benchmark was carried out comparing the GEANT4 and FLUKA simulated proton cross sections to the experimental data from KVI and TOP-IMPLART.

Furthermore, the SEU cross sections of neutrons and protons above 50 MeV are considered to be identical in the JEDEC standard [23], above 30 MeV in [30], and assumed to be the same above 20 MeV in the HEH approximation (see Section I). For this reason, proton data are included in the study for comparison to the SEU neutron cross sections.

The Cypress 65 and ISSI memories were modeled with simple geometry, consisting of a $SiO_2$ back end of line (BEOL) and a Si bulk, containing the rectangular parallelepiped (RPP) sensitive volume (SV). Note that this simplified representation of the BEOL is regarded as an important source of uncertainty for intermediate-energy neutron simulations, in which the specific material composition can have a significant impact on the energy deposition distribution. Although the critical charge tends to decrease with technology scaling, a single feature size can assume a wide range of critical charges (order of a few fC) [9], [31], [32]. Moreover, the critical charge depends on the node capacitance and internal voltages of the memory, which are not typically known, thus TCAD simulations are normally performed to estimate its value [31]. The critical charge of these memories was chosen to best fit the simulated cross sections to the broad range of experimental ones, resulting in accordance with typical values of the technology. This approach can hence be referred to as semiempirical.

The ISSI memory was modeled in FLUKA and in the G4SEE tool, with a cubic RPP of 250 nm sides and a $SiO_2$ BEOL thickness of 6 μm. In the former, 100 RPPs were disposed (to reduce the simulation time) in a matrix $10 \times 10$ inside a bulk structure of $24.5 \times 24.5 \times 0.35$ $\mu m^3$, while in G4SEE a single RPP was employed with the same bulk dimensions. The beam dimensions were covering the whole surface of $24.5 \times 24.5$ $\mu m^2$. The SEU cross section is consequently retrieved through the collected charge inside the SV, considering a critical charge $Q_c$ of 0.72 fC, to be coherent with the FLUKA model of the same memory from [2]. The deposited energy to critical charge conversion is performed considering the factor of 22.5 MeV/pC. The simulated FLUKA and G4SEE proton SEU cross sections are calculated and shown in Fig. 11, together with the proton experimental data. In the same graph, the neutron measurements and G4SEE simulations are reported, also for comparing the data above 30 MeV with the proton SEU cross sections. In addition, the G4SEE simulated neutron SEU cross sections at 50, 100, 150, and 200 MeV are included.

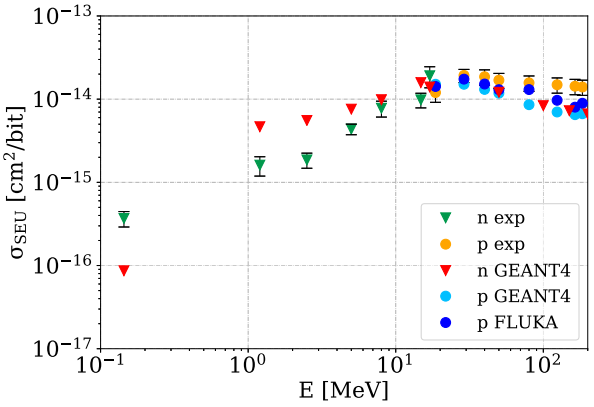


Fig. 11. ISSI 40 nm proton (p) and neutron (n) simulations and experimental data comparison. Proton simulations derive from FLUKA and GEANT4 tools, while the neutron ones from the latter.

Regarding protons, the G4SEE cross sections are compatible within the uncertainty to the experimental data from 18.6 to 50 MeV. At higher energies, the agreement is less satisfactory up to 54% of underestimation by the simulation at 184 MeV. Also, the FLUKA model underestimates the proton cross section at high energy up to 44% and has a good agreement below 80 MeV. The difference between the two Monte Carlo tools may be attributed to the implemented physical models.

For neutrons, instead, G4SEE overestimates, in general, the experimental data, by up to 70% between 17 and 5 MeV. The overestimation is a factor of 3 at low energies (2.5 and 1.2 MeV), while the simulation underestimates the experimental value by 70% at 0.144 MeV. The ISSI neutron cross section simulated at 17 MeV is $1.4 \cdot 10^{-14}$ cm$^2$/bit, compatible with the high-energy proton saturation value rather than with the 17 MeV measurement. The proton SEU cross sections measured and simulated at 18.6 MeV are also compatible with the neutron cross sections at 14 and 17 MeV, showing that proton and neutron cross sections at intermediate energies are still very similar.

Similarly, the Cypress 65 memory was modeled with a cubic RPP of 510 nm side, BEOL thickness of 10 μm, and $Q_c$ of 0.64 fC. These parameters and dimensions were defined on the basis of the ISSI memory model, which exhibits a similar response, and as the technological node of the Cypress is larger, the RPP is also assumed to be larger. As can be noticed, the critical charge of the Cypress 65 nm memory resulted slightly lower than that of the ISSI 40 nm memory, but as anticipated a single feature size can assume a range of critical charges.

The proton and neutron G4SEE simulations are shown in Fig. 12, along with the experimental data. Again, at high proton energies, the simulations underestimate the measure-

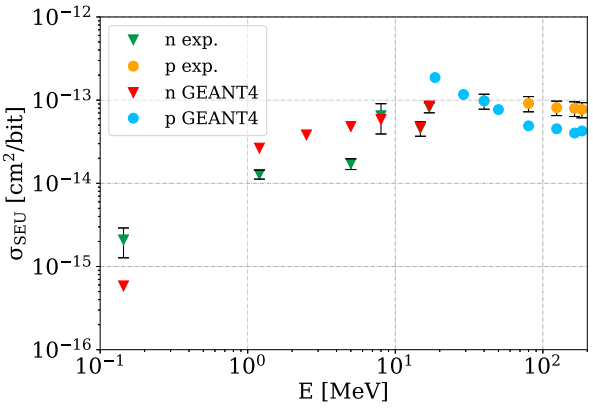


Fig. 12. Cypress 65 nm proton (p) and neutron (n) simulations and experimental data comparison. Proton and neutron simulations derive from GEANT4.

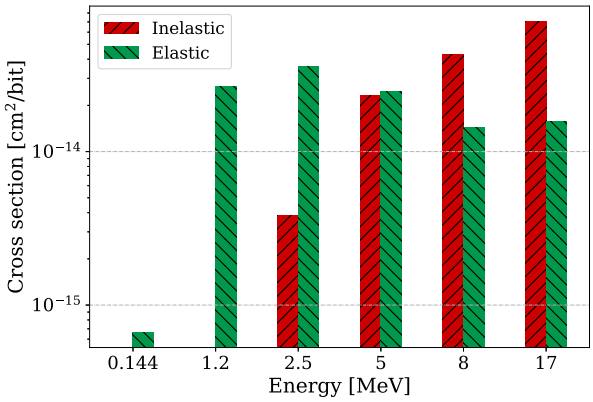


Fig. 13. Elastic and inelastic contributions on the SEU cross section in the Cypress 65 nm memory at varying neutron energy (from GEANT4 simulations).

ments up to 50%. The agreement with neutrons is very good (within 10%) between 8 and 17 MeV. The 5–1.2 MeV are overestimated by the simulations almost a factor of 3 and the 0.144 MeV cross section underestimated by 72%.

Considering the measurement uncertainties (around 20% or higher), the simplified model of the memory and the energy range of several orders of magnitude in which the RPP model is evaluated, the agreement can be considered as satisfactory. Note that these simulations were not intended to perfectly fit the experimental data, as the main objective was to verify the possibility of inducing SEUs with low-energy neutrons. In fact, even considering the memory only composed of Si and $SiO_2$, without taking into account materials of metal layers, plugs, and other insulators, neutrons are shown to be capable of indirectly depositing enough energy to trigger SEUs. This observation supports that the measured SEU cross sections below 2.5 MeV are actually due to neutron interactions. As a conclusion, simulations show compatible results to the experimental data, as well as the difficulty in having a single model capable of reproducing the SEU cross sections for the broad range of energies and particle species.

Moreover, it is worth noting that the systematic overestimation of both RPP models of a factor 2–3 with respect to the data in the 1.2–5 MeV neutron range could be attributed to an over-representation of the oxygen content in the BEOL, considered as pure $SiO_2$. Indeed, being a relatively light atom with respect to other BEOL constituents (Si, Al, Cu), a larger energy can be transferred to oxygen in elastic interactions.

While the lowest energy threshold for an inelastic interaction of neutrons and $^{28}$Si is 2.75 MeV, the deposited energy at lower energies is mainly due to elastic scattering, and the two contributions in G4SEE can be disentangled. The elastic and inelastic contributions to the SEU cross section (absolute values) in the Cypress 65 nm memory are shown in Fig. 13, calculated through GEANT4 at varying neutron energy. It is remarkable to observe how inelastic reactions increase with increasing neutron energy, while elastic processes increase with decreasing neutron energy from 17 to 2.5 MeV. For lower energies, the collected charge to trigger an SEU is only provided by elastic collisions. Moreover, until 5 MeV, SEUs are mainly due to elastic collisions, while with higher energies, the inelastic interactions are more effective.

As the simplified geometry of the simulation consists in silicon and oxygen, the energy can be transferred only to these atoms. The maximum energy transferred from a neutron during an elastic collision is given by the following equation:

$$E_{\max} = E_n \cdot \frac{4A}{(A+1)^2}. \tag{2}$$

Here, $E_n$ is the energy of the incoming neutron and $A$ is the mass number of the target atom. For instance, considering the 144 keV case, the maximum elastic energy transferred by a neutron in silicon ($A = 28$) is 19 keV, while in oxygen ($A = 16$), it is 32 keV. Therefore, most of the deposited energy will result from elastic scattering with oxygen, and more in general with the lighter nucleus. The corresponding maximum deposited charge in silicon and oxygen is 0.84 and 1.42 fC, respectively. Both are above the critical charge for the ISSI and Cypress 65 models, and therefore also from a calculation point of view, elastic scattering from 144 keV neutrons is thought to be capable of depositing sufficient charge to trigger an SEU. Note, however, that the nuclear stopping power for such low energies, which is negligible compared to the electronic stopping power at higher energies, can have a significant impact on the total energy deposition. The GEANT4 simulations include both contributions.

## VIII. Conclusion

Neutrons in the 0.1–10 MeV energy range can play a critical role in inducing SEUs in nm technologies. As shown with a 65 nm SRAM, the neutron cross section at 1.2 MeV is only six times lower than its saturation value, while for previously studied components, it is typically on the order of hundreds of times lower. A similar behavior was observed for a 40 nm memory. The SER induced by neutrons in the 0.1–10 MeV interval can be up to 63% the overall rate in accelerator environments. At ground level the rate is up to 16%, while for avionic applications at 12 km of altitude it can reach up to 19%, therefore representing a possible threat for high-reliability systems. Even neutrons between 0.1 and 3 MeV, which resulted negligible in previous studies,

can yield a significant impact on the SER, up to 44% in accelerator environments. Moreover, though not covered in this work, the higher SEU cross section of integrated technologies in the 0.1–10 MeV range is expected to have a significant impact on SER in environments with less energetic neutron spectra than the atmospheric or accelerator ones, such as fission/fusion, or medical.

GEANT4 simulations support the experimental response shape of the memories and the possibility of inducing SEEs even with neutrons of 144 keV due to elastic collisions, showing also that neutron and proton SEU cross sections are compatible above 20 MeV. However, the choice of the RPP model dimensions and critical charge to describe a memory is not straightforward, especially when the model has to reproduce both the neutron and proton SEU cross sections ranging several orders of magnitude. Moreover, the package of the memory does not significantly impact the neutron SEU cross section, as experimentally measured. An Am–Be source was used to further validate the intermediate neutron response shape of the devices and the effects of the package.

Moreover, it is shown that the HEHeq standard response used at CERN to estimate the SER of electronics can result in underestimations of up to a factor 2. This underestimation would be larger for accelerator environments with softer spectra than that considered in the analysis. Consequently, three possible RHA solutions are presented.

Finally, SEUs can still be induced even below the so far considered threshold of 0.2 MeV in the HEHEeq fluence calculation, although their contribution to the overall rate is below 4%.

## REFERENCES


[1] K. Roeed *et al.*, "Method for measuring mixed field radiation levels relevant for SEEs at the LHC," *IEEE Trans. Nucl. Sci.*, vol. 59, no. 4, pp. 1040–1047, Aug. 2012.

[2] R. G. Alia *et al.*, "Direct ionization impact on accelerator mixed-field soft-error rate," *IEEE Trans. Nucl. Sci.*, vol. 67, no. 1, pp. 345–352, Jan. 2020.

[3] M. Cecchetto, R. G. Alia, S. Gerardin, M. Brugger, A. Infantino, and S. Danzeca, "Impact of thermal and intermediate energy neutrons on SRAM SEE rates in the LHC accelerator," *IEEE Trans. Nucl. Sci.*, vol. 65, no. 8, pp. 1800–1806, Aug. 2018.

[4] J. Baggio, D. Lambert, V. Ferlet-Cavrois, P. Paillet, C. Marcandella, and O. Duhamel, "Single event upsets induced by 1–10 MeV neutrons in static-RAMs using mono-energetic neutron sources," *IEEE Trans. Nucl. Sci.*, vol. 54, no. 6, pp. 2149–2155, Dec. 2007.

[5] D. Lambert *et al.*, "Single event upsets induced by a few MeV neutrons in SRAMs and FPGAs," in *Proc. IEEE Radiat. Effects Data Workshop (REDW)*, Jul. 2017, pp. 114–118.

[6] H. Quinn, A. Watkins, L. Dominik, and C. Slayman, "The effect of 1–10-MeV neutrons on the JESD89 test standard," *IEEE Trans. Nucl. Sci.*, vol. 66, no. 1, pp. 140–147, Jan. 2019.

[7] B. D. Sierawski *et al.*, "Contribution of low-energy ($< 10$ MeV) neutrons to upset rate in a 65 nm SRAM," in *Proc. IEEE Int. Rel. Phys. Symp.*, May 2010, pp. 395–399.

[8] M. Cecchetto *et al.*, "SEE flux and spectral hardness calibration of neutron spallation and mixed-field facilities," *IEEE Trans. Nucl. Sci.*, vol. 66, no. 7, pp. 1532–1540, Jul. 2019.

[9] G. Hubert and L. Artola, "Experimental evidence of ground albedo neutron impact on soft error rate for nanoscale devices," *IEEE Trans. Nucl. Sci.*, vol. 66, no. 1, pp. 262–269, Jan. 2019.

[10] G. Hubert and L. Artola, "Study of secondary scattering/albedo neutron fields and their impacts on SER as function of scene topologies," *IEEE Trans. Nucl. Sci.*, vol. 67, no. 1, pp. 201–209, Jan. 2020.

[11] H. J. Brede *et al.*, "The Braunschweig accelerator facility for fast neutron research: 1: Building design and accelerators," *Nucl. Instrum. Meth.*, vol. 169, no. 3, pp. 349–358, 1980.

[12] A. Pietropaolo *et al.*, "The Frascati neutron generator: A multipurpose facility for physics and engineering," *J. Phys., Conf. Ser.*, vol. 1021, May 2018, Art. no. 012004, doi: 10.1088/1742-6596/1021/1/012004.

[13] L. Picardi *et al.*, "Beam commissioning of the 35 MeV section in an intensity modulated proton linear accelerator for proton therapy," *Phys. Rev. A, Gen. Phys. Accel. Beams*, vol. 23, no. 2, Feb. 2020, Art. no. 020102.

[14] E. R. van der Graaf, R. W. Ostendorf, M.-J. van Goethem, H. H. Kiewiet, M. A. Hofstee, and S. Brandenburg, "AGORFIRM, the AGOR facility for irradiations of materials," in *Proc. Eur. Conf. Radiat. Effects Compon. Syst.*, Sep. 2009, pp. 451–454.

[15] D. Lambert *et al.*, "Analysis of quasi-monoenergetic neutron and proton SEU cross sections for terrestrial applications," *IEEE Trans. Nucl. Sci.*, vol. 53, no. 4, pp. 1890–1896, Aug. 2006.

[16] R. Nolte and D. J. Thomas, "Monoenergetic fast neutron reference fields: I. Neutron production," *Metrologia*, vol. 48, no. 6, pp. S263–S273, Oct. 2011.

[17] S.-I. Abe *et al.*, "Impact of hydrided and non-hydrided materials near transistors on neutron-induced single event upsets," in *Proc. IEEE Int. Rel. Phys. Symp. (IRPS)*, Apr. 2020, pp. 8C.5.1–8C.5.7.

[18] J. Beaucour *et al.*, "Grenoble large scale facilities for advanced characterisation of microelectronics devices," in *Proc. 15th Eur. Conf. Radiat. Effects Compon. Syst. (RADECS)*, Sep. 2015, pp. 312–315.

[19] G. Battistoni *et al.*, "Overview of the FLUKA code," *Ann. Nucl. Energy*, vol. 82, pp. 10–18, Aug. 2015.

[20] T. T. Böhlen *et al.*, "The FLUKA code: Developments and challenges for high energy and medical applications," *Nucl. Data Sheets*, vol. 120, pp. 211–214, Jun. 2014.

[21] V. Vlachoudis, "FLAIR: A powerful but user friendly graphical interface for FLUKA," in *Proc. Int. Conf. Math., Comput. Meth. React. Phys.*, Saratoga Springs, NY, USA, 2009, pp. 1–11.

[22] M. Cecchetto, "Impact of thermal and intermediate energy neutrons on the semiconductor memories for the CERN high-energy accelerators," M.S. thesis, Dept. Inf. Eng., Univ. Padova, Padua, Italy, Jul. 2017.

[23] *Measurement and Reporting of Alpha Particle and Terrestrial Cosmic Ray-Induced Soft Errors in Semiconductor Devices*, Standard JESD89A, JEDEC, Oct. 2006.

[24] M. Cecchetto, R. G. Alía, and F. Wrobel, "Impact of energy dependence on ground level and avionic SEE rate prediction when applying standard test procedures," *Aerospace*, vol. 6, no. 11, p. 119, Nov. 2019.

[25] J. Mekki, M. Brugger, R. G. Alia, A. Thornton, N. C. D. S. Mota, and S. Danzeca, "CHARM: A mixed field facility at CERN for radiation tests in ground, atmospheric, space and accelerator representative environments," *IEEE Trans. Nucl. Sci.*, vol. 63, no. 4, pp. 2106–2114, Aug. 2016.

[26] M. Cecchetto *et al.*, "Thermal neutron-induced SEUs in the LHC accelerator environment," *IEEE Trans. Nucl. Sci.*, vol. 67, no. 7, pp. 1412–1420, Jul. 2020.

[27] J. Allison *et al.*, "Recent developments in Geant4," *Nucl. Instrum. Meth. Phys. Res. Sect. A, Accel., Spectrometers, Detect. Assoc. Equip.*, vol. 835, pp. 186–225, Nov. 2016. [Online]. Available: http://www.sciencedirect.com/science/article/pii/S0168900216306957

[28] Geant4 Collaboration. (Dec. 2019). *Geant4 Guide For Physics Lists, Release 10.6, Rev4.0*. [Online]. Available: http://cern.ch/geant4-userdoc/UsersGuides/PhysicsListGuide/BackupVersions/V10.6/fo/PhysicsListGuide.pdf

[29] Geant4 Collaboration. (Dec. 2019). *Geant4 Physics Reference Manual, Release 10.6, Rev4.0*. [Online]. Available: http://cern.ch/geant4-userdoc/UsersGuides/PhysicsReferenceManual/BackupVersions/V10.6/fo/PhysicsReferenceManual.pdf

[30] D. Lambert, F. Desnoyers, and D. Thouvenot, "Investigation of neutron and proton SEU cross-sections on SRAMs between a few MeV and 50 MeV," in *Proc. Eur. Conf. Radiat. Effects Compon. Syst.*, Sep. 2009, pp. 148–154.

[31] R. Naseer, Y. Boulghassoul, J. Draper, S. DasGupta, and A. Witulski, "Critical charge characterization for soft error rate modeling in 90 nm SRAM," in *Proc. IEEE Int. Symp. Circuits Syst.*, May 2007, pp. 1879–1882.

[32] S.-I. Abe and Y. Watanabe, "Analysis of charge deposition and collection caused by low energy neutrons in a 25-nm bulk CMOS technology," *IEEE Trans. Nucl. Sci.*, vol. 61, no. 6, pp. 3519–3526, Dec. 2014.